AIP Advances

A redefined energy functional to prevent mass loss in phase-field methods

Cite as: AIP Advances **10**, 065124 (2020); https://doi.org/10.1063/1.5142353
Submitted: 12 December 2019 . Accepted: 27 May 2020 . Published Online: 16 June 2020

M. Kwakkel, M. Fernandino, and C. A. Dorao

A redefined energy functional to prevent mass loss in phase-field methods

Cite as: AIP Advances 10, 065124 (2020); doi: 10.1063/1.5142353
Submitted: 12 December 2019 • Accepted: 27 May 2020 •
Published Online: 16 June 2020

M. Kwakkel,[a] M. Fernandino,[b] and C. A. Dorao

AFFILIATIONS

Department of Energy and Process Engineering, Norwegian University of Science and Technology, 7491 Trondheim, Norway

[a]Author to whom correspondence should be addressed: marcel.kwakkel@ntnu.no
[b]Electronic mail: maria.fernandino@ntnu.no

ABSTRACT

Phase-field modeling has gained considerable attention for the study of two-phase systems. The method consists of introducing a field that can represent the state of matter or the atomic species concentration. In this way, the fields identify locally the phase present at a given point and also the location of interfaces. However, a well-known limitation of phase-field methods is (enclosed) mass loss and bulk diffusion, which has motivated numerous approaches in order to counteract these issues. In this work, it is shown that both issues can be attributed to a nonphysical term originating from the definition of the energy functional, which causes mass change by mean curvature. Therefore, a redefined energy functional is presented, which ensures a proper energy balance. While avoiding the nonphysical bulk diffusion, it achieves conservation of (enclosed) mass as well. Furthermore, overall system dynamics remain comparable to the classic energy functional. The redefined energy potential is still able to model spinodal decomposition, while it matches sharp interface results better when applied to a two-phase system.

I. INTRODUCTION

The phase-field method has emerged as a popular approach for the modeling of systems involving two phases. Its ability to include micro-scale interface physics in the energy formulation while maintaining a relatively easy implementation makes it a powerful and promising way toward the simulation of more complex physical phenomena. It has been used for modeling a wide range of two-phase systems, such as detailed interface dynamics,[1–5] turbulent two-phase flows,[6,7] binary alloys,[8–10] thermo-capillary flows,[11,12] and phase change.[13–15]

The phase-field method is based on a diffuse interface description suggested by van der Waals[16] more than a century ago and extended later by Cahn and Hilliard.[8,17,18] These models provide an expression for determining the properties of the system across a flat interface between two coexisting phases. This approach was later extended to allow the simulation of phase separation by spinodal decomposition in multiple dimensions.[19,20] However, this extension also introduced mass conservation issues like spontaneous shrinkage of drops[21] and assimilation of smaller drops by larger ones (coarsening).[22] Since nonphysical, a substantial amount of studies have tried to remedy these mass conservation issues by various approaches: selection of optimal parameters, introduction of Lagrange multipliers,[23–26] addition of correction terms,[7,27–29] application of a re-initialization process,[30] and adaptive grid techniques to increase the interfacial grid resolution.[31] Although some of these remedies appear to work well, so far no theoretical cause for the mass conservation issues themselves has been put forward.[32] Moreover, the occurrence of this nonphysical interface motion and mass diffusion has been denoted as an important limitation of phase-field methods.[33]

The phase-field model for a two-phase system is based on the definition of a phase-field parameter C, which attains values between $C = 0$ and $C = 1$.[34] Away from the interface, C attains these limiting values, while there is a smooth transition between these limiting values around the interface. A phase-field method defines an energy functional that is commonly the following Helmholtz (free) energy functional,

$$\mathcal{F} = \int_\Omega f \, \mathrm{d}V = \int_\Omega \frac{\sigma}{\epsilon}\left(\Psi(C) + \frac{\epsilon^2}{2}(\nabla C)^2\right)\mathrm{d}V, \tag{1}$$

where f is the Helmholtz energy density, σ denotes the surface tension coefficient, and ϵ determines the width of the diffuse interface.

The two terms in the energy functional account for the bulk energy density and the excess energy due to an inhomogeneous distribution of C in the interfacial region, respectively. The phobic bulk energy density $\Psi(C)$ is a double-well potential, which can be written as $\Psi(C) = 1/4C^2(1-C)^2$. This double-well potential has minima at $C = 0$ and $C = 1$ and tries to sharpen the interface by separating the phases. On the other hand, the philic gradient term tries to diffuse the interface into the bulk regions. At minimum energy, both terms balance, and the interface profile reaches its equilibrium shape. It is important to note that the original works by van der Waals[16] and Cahn and Hilliard[8,17,18] correspond to a one dimensional case (thereby assuming a flat interface). In that case, it holds that $\nabla C = dC/dz$ and $\Delta C = d^2C/dz^2$, where z is a spatial location. In this work, it is shown that the extension of the latter term to higher dimensions can cause mass conservation issues, which can be prevented by a redefinition of the energy functional.

II. GOVERNING EQUATIONS

Incompressible fluid flows are governed by continuity and momentum equations, commonly known as the Navier–Stokes equations. By solving these equations, the velocity and pressure fields within the flow domain are obtained. Immiscible two-phase flows are characterized by the presence of an interface, which in phase-field methods is implicitly defined by the phase-field parameter C. The phase-field equation provides the evolution of C, which can also be advected by the velocity field. Meanwhile, as density, viscosity, and surface tension depend on the location of the interface, the Navier–Stokes equations depend on the phase-field parameter C. Therefore, by coupling the Navier–Stokes and phase-field equations, the evolution of an immiscible two-phase system can be studied numerically.

A. Navier–Stokes equations

Consider a two-phase fluid system, where the phases are denoted by 0 and 1. If both fluid phases are isothermal incompressible Newtonian fluids, their motion can be described by the following continuity and momentum equations:

$$\nabla \cdot \mathbf{u} = 0, \tag{2}$$

$$\rho \frac{\partial \mathbf{u}}{\partial t} + \mathbf{u} \cdot \nabla \mathbf{u} = -\nabla p + \nabla \cdot \tau + \mathbf{f_b} + \mathbf{f_{st}}, \tag{3}$$

where $\mathbf{u}$ denotes the velocity vector, p the pressure, $\tau = \mu\left(\nabla \mathbf{u} + (\nabla \mathbf{u})^T\right)$ the viscous stress tensor, $\mathbf{f_b}$ any body forces, such as gravity, and $\mathbf{f_{st}}$ the surface tension force. The density ρ and viscosity μ are functions of C,

$$\rho = \rho_0(1-C) + \rho_1 C, \tag{4}$$

$$\mu = \mu_0(1-C) + \mu_1 C, \tag{5}$$

which shows that $\rho = \rho_0$ and $\mu = \mu_0$ if $C = 0$ and $\rho = \rho_1$ and $\mu = \mu_1$ if $C = 1$. At the interface Γ, the following kinematic and dynamic conditions hold,

$$[\mathbf{u}]_\Gamma = 0, \tag{6}$$

$$[(-p + \tau) \cdot \mathbf{n}]_\Gamma = -\sigma \kappa_\Gamma \mathbf{n}_\Gamma, \tag{7}$$

where $[\cdot]_\Gamma$ denotes a jump across the interface Γ, σ is the surface tension coefficient, κ_Γ is the curvature of the interface, and $\mathbf{n}_\Gamma$ is the interface normal vector (which points from phase 0 to phase 1 and is defined by $\mathbf{n}_\Gamma = \nabla C/|\nabla C|$). As the phase-field parameter C represents the interface by a smooth continuous function, according to Eq. (5), also, the viscosity will be continuous across the interface. Kang, Fedkiw, and Liu[35] showed that in that case, the pressure jump across the interface is decoupled from the velocity field, and Eqs. (6) and (7) reduce to

$$[\nabla \mathbf{u}]_\Gamma = 0, \tag{8}$$

$$[p]_\Gamma = \sigma \kappa_\Gamma. \tag{9}$$

Following the Continuous Surface Force (CSF) method,[36] the sharp curvature κ_Γ can be smoothened. This leads to the following relation for the surface tension force:

$$\mathbf{f}_{st} = \sigma \kappa_\Gamma |\nabla C|. \tag{10}$$

B. Phase-field equation

In practice, the equilibrium phase-field C can be written in terms of the signed distance function $d(\mathbf{x})$ between the interface and the location $\mathbf{x}$, i.e.,

$$C(\mathbf{x}) = \frac{1}{2} + \frac{1}{2}\tanh\left(\frac{d(\mathbf{x})}{2\sqrt{2}\epsilon}\right). \tag{11}$$

The evolution of this phase-field $C(\mathbf{x}, t)$ is mathematically given by the following conservation equation:

$$\frac{\partial C}{\partial t} + \nabla \cdot (\mathbf{u}C) = -\nabla_{\mathcal{H}} f(C), \tag{12}$$

where the advection is controlled by the fluid velocity $\mathbf{u}$, and the right-hand side is given by a so-called gradient flow of the energy density $f(C)$. For $\mathbf{u} = 0$, the uncoupled (from the NS equation) phase-field equation is obtained, where the evolution of C is only affected by the term on the right-hand side. Here, $\nabla_{\mathcal{H}}$ denotes the (Hilbert space) gradient of f at C, which ensures that C decreases along the gradient of f on $\mathcal{H}$. The precise expression for $\nabla_{\mathcal{H}}$ can be found from a thermodynamic perspective[37] or by a variational formulation (see Appendix A). Two well-known results are the Allen–Cahn (AC) equation (so-called L^2 gradient flow),

$$\frac{\partial C}{\partial t} + \nabla \cdot (\mathbf{u}C) = -M_A \omega, \tag{13}$$

and the Cahn–Hilliard (CH) equation (so-called H^{-1} gradient flow),

$$\frac{\partial C}{\partial t} + \nabla \cdot (\mathbf{u}C) = \nabla \cdot (M_C \nabla \omega). \tag{14}$$

Here, M is the interface mobility (often set to unity or a function of C), ω the chemical potential, and the subscripts A and C denote Allen–Cahn and Cahn–Hilliard, respectively. The commonly used chemical potential ω_c, where c signifies the classic approach, is given by the functional derivative of the energy density Eq. (1) with respect to the phase-field C,

$$\omega_c = \frac{\partial f}{\partial C} = \frac{\sigma}{\epsilon}\left(\frac{\partial \Psi}{\partial C} - \epsilon^2 \Delta C\right), \tag{15}$$

which reduces to

$$\omega_c = \frac{\sigma}{\epsilon}\left(C^3 - \frac{3}{2}C^2 + \frac{1}{2}C - \epsilon^2\Delta C\right). \tag{16}$$

C. Mass conservation requirements

The amount of mass within a domain is defined by the volume integral of C over it. Therefore, the mass within a (constant volume) domain Ω is conserved if

$$\frac{\partial}{\partial t}\int_\Omega C\,\mathrm{d}V = \int_\Omega \frac{\partial C}{\partial t}\,\mathrm{d}V = 0 \quad \forall\, t. \tag{17}$$

Next, by taking the volume integral of Eq. (12), a mass balance is obtained. By Gauss's theorem, the advection term in this equation can be converted from a volume integral over Ω into a surface integral over its closed boundary $\partial\Omega$,

$$\int_\Omega \nabla\cdot(\mathbf{u}C)\,\mathrm{d}V = \oint_{\partial\Omega} C(\mathbf{u}\cdot\mathbf{n}_s)\,\mathrm{d}S, \tag{18}$$

where $\mathbf{n}_s$ is the surface normal vector of $\partial\Omega$. The latter relation becomes zero if there is no net inflow or outflow over the boundary $\partial\Omega$. This is generally achieved by a no penetration boundary condition $\mathbf{u}\cdot\mathbf{n}_s = 0$ on $\partial\Omega$. It follows from Eqs. (13) and (14) that by enforcing

$$\int_\Omega M_A\omega\,\mathrm{d}V = 0 \quad \forall\, t \qquad \text{for AC}, \tag{19}$$

$$\oint_{\partial\Omega} M_C\nabla\omega\cdot\mathbf{n}_s\,\mathrm{d}S = 0 \quad \forall\, t \qquad \text{for CH}, \tag{20}$$

mass will be conserved. Here, Gauss's theorem has been applied again to the CH equation to convert the volume integral over Ω into a surface integral over its closed boundary $\partial\Omega$. The first relation shows that the AC method conserves mass if the volume integral of $M_A\omega$ over Ω remains zero in time. In practice, this integral condition is difficult to maintain, as it cannot be enforced by a local condition for $M_A\omega$. The second relation shows that the CH method conserves mass if the volume integral of $M_C\nabla\omega\cdot\mathbf{n}_s$ remains zero in time. For a general M_C, this can be ensured by setting $\nabla\omega\cdot\mathbf{n}_s = 0$ on $\partial\Omega$. Some studies have tried to adapt the interface mobility M_C to ensure the total and enclosed mass conservation. This is possible as long as the interface mobility M_C remains zero on $\partial\Omega$. However, as the interface mobility must also be nonzero around the interface, enforcing $M_C = 0$ on $\partial\Omega$ will in general lead to strong gradients in M_C around $\partial\Omega$ (which in turn might increase numerical errors). Therefore, the main focus of this work is on the definition of the chemical potential.

Next, consider Ω to be a volume enclosed by the interface Γ, which implies that $\partial\Omega = \Gamma$. Therefore, identical conditions should hold for the conservation of enclosed mass. However, as the interface Γ is an implicit boundary, where $\nabla\omega\cdot\mathbf{n}_\Gamma$ might become nonzero, conservation of interface enclosed mass is not automatically assured for general M_C. In particular, the classic chemical potential of Eq. (16) breaks this condition for curved interfaces.

D. Redefined energy functional

The dynamics of the original one-dimensional formulation is governed by a balance between a phobic bulk energy density term (interface sharpening) and a philic gradient term (interface diffusing). At minimum energy, both terms balance, and the interface profile reaches its equilibrium shape. The extension to higher dimensions of the chemical potential is given by Eq. (16), which is commonly used without question. As intended, when applied to one-dimensional problems, this chemical potential enforces the balance between the sharpening and diffusing terms while conserving (enclosed) mass. At the same time, it is well known that this chemical potential can cause nonphysical (enclosed) mass loss and bulk diffusion when applied to higher-dimensional problems. Therefore, a substantial amount of studies have tried to remedy these nonphysical effects in various ways.[7,23–31] Although some of these remedies appear to suppress the nonphysical effects, so far no theoretical cause and prevention of them has been put forward.[32] However, it is possible to attribute the (enclosed) mass loss and bulk diffusion directly to the extension of the original one-dimensional formulation (corresponding to a flat interface) to higher dimensions.

As derived in Sec. II C, conservation of enclosed mass for general M requires $\nabla\omega\cdot\mathbf{n}_\Gamma \equiv 0$ on the interface Γ. The original one-dimensional formulation by van der Waals[16] and Cahn and Hilliard[8,17,18] does obey this condition and therefore conserves enclosed mass. However, it can be shown that the classic chemical potential ω_c of curved equilibrium interfaces with nonzero thickness does not fulfill this requirement. This same behavior was identified by Yue, Zhou, and Feng[22] based on energy arguments as an inherent property of the CH equation in multiple dimensions when using the classic chemical potential. Starting from the equilibrium interface profile given by (11), the following relations hold (where $\mathbf{x}$ has been omitted for readability):

$$\begin{aligned}
\tanh\left(\frac{d}{2\sqrt{2}\epsilon}\right) &= 2\left(C - \frac{1}{2}\right),\\
\nabla C &= \frac{C(1-C)}{\sqrt{2}\epsilon}\nabla d,\\
\Delta C &= \frac{C(1-C)}{\sqrt{2}\epsilon}\Delta d + \frac{\Psi'(C)}{\epsilon^2}\nabla d^2,
\end{aligned} \tag{21}$$

where $\Psi'(C) = \left(C - \frac{1}{2}\right)C(C-1)$, and ∇ and Δ denote the gradient and Laplacian operators, respectively. As long as $d(\mathbf{x})$ remains a unit distance function, it holds that $|\nabla d| \equiv 1$ and $\partial^2 d/\partial n^2 \equiv 0$. The mean curvature H of an interface is mathematically defined by

$$2H = \frac{\frac{\partial^2 d}{\partial n^2} - \Delta d}{|\nabla d|} = \kappa, \tag{22}$$

which results in $\kappa = -\Delta d$. Next, at equilibrium, the classic chemical potential ω_c of Eq. (16) can be simplified to

$$\begin{aligned}
\omega_c &= \frac{\sigma}{\epsilon}\left(\left(C - \frac{1}{2}\right)C(C-1) - \epsilon^2\Delta C\right),\\
&= \epsilon\sigma\kappa|\nabla C|,\\
&= \sigma\kappa\frac{C(1-C)}{\sqrt{2}},
\end{aligned} \tag{23}$$

where it has been used that

$$|\nabla C| = \frac{C(1-C)}{\sqrt{2}\epsilon}. \tag{24}$$

As the interface normal gradient of the curvature ($\nabla\kappa\cdot\mathbf{n}_\Gamma$) is always nonzero for curved interfaces, consequently for curved interfaces with a thickness $\epsilon > 0$ also $\nabla\omega\cdot\mathbf{n}_\Gamma \neq 0$. Only in the sharp interface limit, when $\epsilon \to 0$ and C becomes identically 0 or 1, this additional nonuniform chemical potential at equilibrium becomes zero. Therefore, it is the curvature embedded in ω_c that causes mass loss and bulk diffusion.

Without loss of generality, it can be assumed that the extension of the energy functional to higher dimensions should consider the gradient of the single phase-field C normal to the interface. The classic Helmholtz energy functional of Eq. (1) is then redefined to

$$\mathcal{F}_b = \int_\Omega f_b \,\mathrm{d}V = \int_\Omega \frac{\sigma}{\epsilon}\left(\Psi(C) + \frac{\epsilon^2}{2}(\nabla_n C)^2\right)\mathrm{d}V, \tag{25}$$

where ∇_n is the gradient normal to the interface. The fundamental difference is that here, $\nabla_n C$ (a scalar) is used, compared to ∇C (a vector) in the classic Helmholtz energy functional. This subtle modification of the energy functional leads to the following balanced chemical potential (see Appendix B for its derivation):

$$\omega_b = \frac{\partial f_b}{\partial C} = \frac{\sigma}{\epsilon}\left(C^3 - \frac{3}{2}C^2 + \frac{1}{2}C - \epsilon^2\frac{\partial^2 C}{\partial n^2}\right), \tag{26}$$

which is identically zero for an interface (profile) at equilibrium [corresponding to Eq. (11)]. It can be shown, through a similar analysis to that used before, that even for curved equilibrium interfaces $\nabla\omega_b\cdot\mathbf{n}_\Gamma \equiv 0$, which proves that the balanced chemical potential does not cause any mass loss and bulk diffusion.

During the derivation of the classic chemical potential Eq. (16), the divergence of ∇C leads to an additional curvature term. This can be understood by considering the difference between the two chemical potentials,

$$\omega_c - \omega_b = -\sigma\epsilon\left(\Delta C - \frac{\partial^2 C}{\partial n^2}\right) = \sigma\kappa\epsilon|\nabla C|, \tag{27}$$

where κ is the curvature. This relation also reflects that mass loss and bulk diffusion for the classic chemical potential only vanish if $\epsilon \to 0$, the so-called sharp interface limit.[21] From a physical perspective, minimization of the redefined Helmholtz energy functional effectuates only the recovery of the equilibrium interface profile. This dynamics corresponds to the original one-dimensional formulation and does in general not depend on the interface thickness ϵ. On the other hand, minimization of the classic Helmholtz energy functional effectuates a balance between the recovery of the equilibrium interface profile and a uniform distribution of the right-hand side term of Eq. (27). However, neither of these goals is accomplished completely, and the overall dynamics strongly depends on the interface thickness ϵ. This can be understood better by combining the difference between the chemical potentials (27) with the uncoupled (from the NS equation) CH equation (14). For a curved interface with an equilibrium hyperbolic tangent profile and constant M_C, this gives

$$\frac{\partial C}{\partial t} = M_C\sigma\epsilon\Delta(\kappa|\nabla C|), \tag{28}$$

which shows that, in order to make $\kappa|\nabla C|$ more uniform in space, C (and therefore the hyperbolic tangent interface profile) will change. Based on Eq. (10), $\kappa|\nabla C|$ can be considered as a pressure jump across (or a surface tension force at) the interface in the normal direction. From a physical perspective, this interface normal (pressure) term is balanced by surface tension forces parallel to the interface (through the Young–Laplace equation) and must not be diffused. Therefore, as the use of this additional diffusion term is physically problematic, it should be removed. The proposed balanced chemical potential does just that, while respecting the original one-dimensional dynamics. As the multi-dimensional balanced energy functional is essentially identical to the one-dimensional version, application of the energy argument[22] yields an equilibrium for the hyperbolic tangent profile given by Eq. (11) without any need for droplet shrinkage. Moreover, by removing the source of the mass loss and bulk diffusion, the need for correction terms or special settings has vanished.

III. NUMERICAL RESULTS

To validate the effect of both chemical potentials in combination with the CH equation (14), three 2D benchmark cases are presented. All cases are simulated with an in-house C^1 continuous least-squares spectral element method, which allows the use of adaptive mesh refinement.[38,39] Unless stated otherwise, in each spatial direction, six modes (fifth order C^1 Hermite polynomials) are used. Integral expressions are numerically approximated by Gaussian quadrature based on seven Gauss–Lobatto–Legendre roots in each spatial direction. Nonlinear convergence is declared once the relative norm of the residual is below 10^{-4}. For two-phase simulation, it is common to couple the NS and CH equations, as described in Sec. II. However, to emphasize that results strongly depend on the phase-field equation alone, for the first two problems, no coupling with any velocity field is assumed. First, a static circular interface initialized from the equilibrium interface profile given by Eq. (11) is presented. It demonstrates that the classic chemical potential ω_c, in contrast to the balanced chemical potential ω_b, causes mass loss and bulk diffusion. Next, to illustrate how both chemical potentials perform dynamically, a spinodal decomposition is presented. It visualizes how the whole system is affected by the choice of chemical potential and allows a discussion on their consequences for interface dynamics. The final case is the rise of a buoyant bubble, for which the coupled NSCH equations are solved. The simulation results are validated with available sharp interface results.

A. Stationary droplet

In Fig. 1, a static circular interface with radius $R = 1$ on a $[4 \times 4]$ square domain with Neumann boundary conditions is considered. This square domain is divided into 8×8 spectral elements, and the adaptive mesh refinement will refine the mesh two times around the interface. To amplify any mass issues, the interface thickness is set to a relatively high value of $\epsilon = 0.08$, and $M = 1$ is used. Once the solution reaches a steady state (uniform ω), the simulation is stopped. Even though the interface is initialized from the equilibrium profile given by Eq. (11), Fig. 1(c) shows that the classic chemical potential is initially nonuniform in space. Moreover, because the maximum of the chemical potential does not coincide with the interface location exactly, according to Eq. (20), mass changes will occur. It will lead to the loss of enclosed mass (here, almost 9%) and bulk diffusion, as shown in Figs. 1(a) and 1(b), respectively. As the balanced chemical

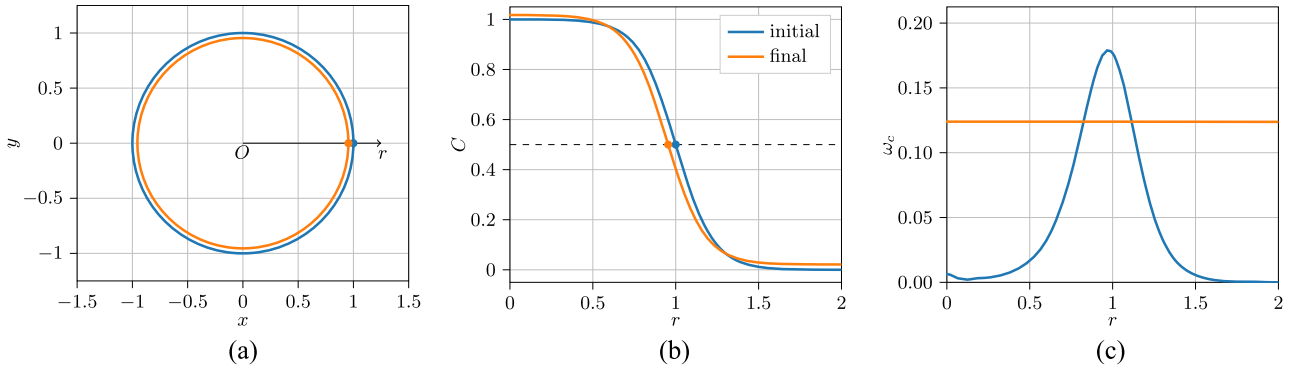

FIG. 1. Depiction of the dynamics of a circular drop from the initial hyperbolic tangent profile toward a final steady state profile if the classic chemical potential is applied. Note that since the balanced chemical potential is already identically zero for the initial hyperbolic tangent profile, it does not affect the initial interface location and profile. (a) Top view of the interface location, which shows that the initial enclosed region decreases until the steady state. (b) Profile of C along the radius, which shows a clear bulk diffusion far from the interface that moves the interface (dot). (c) Profile of the classic chemical potential ω_c along the radius, at the steady state, it has become uniform in space.

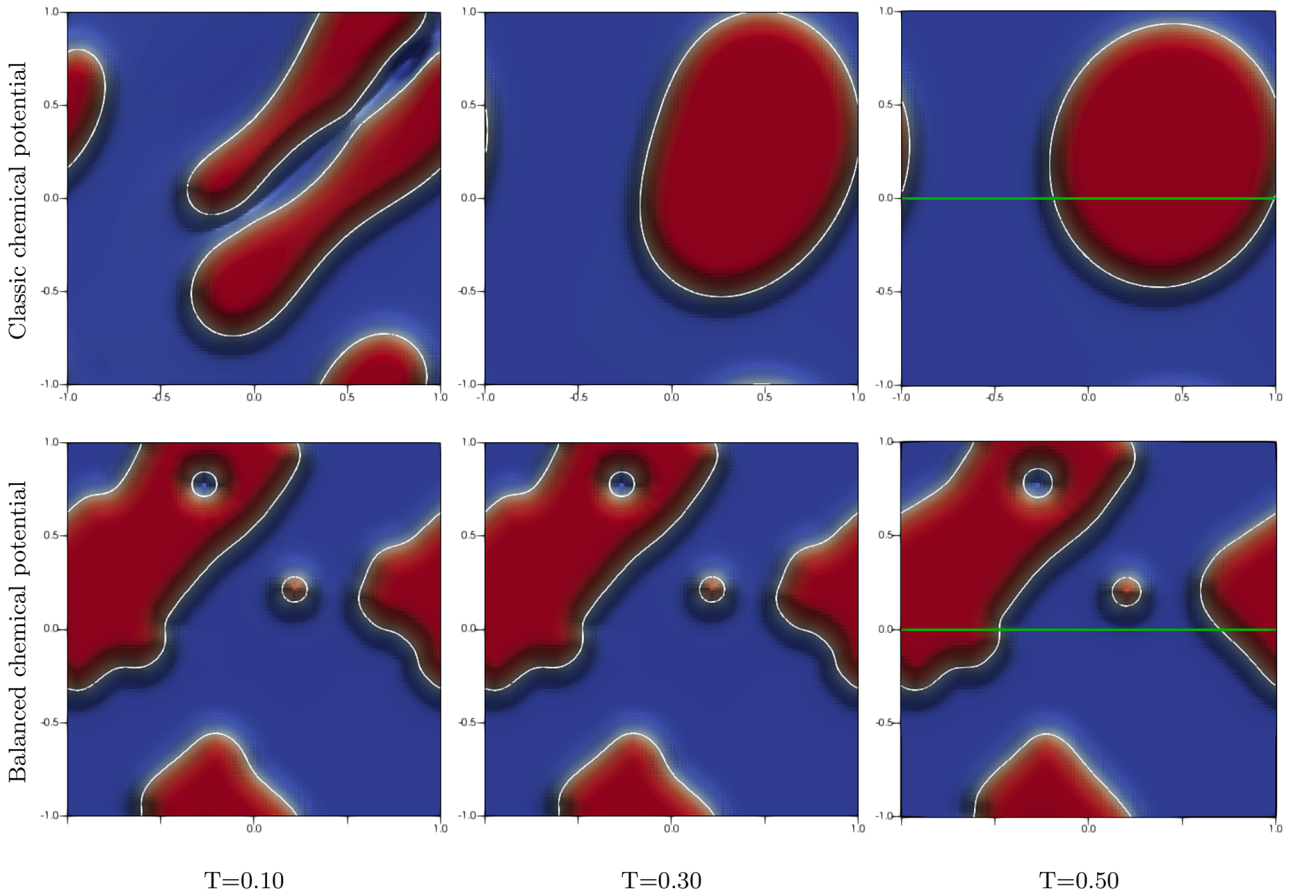

FIG. 2. Spinodal decomposition for two different chemical potentials at different time levels. The classic chemical potential (top) performs diffusion by mean curvature and therefore always leads to a single circular interface ($C \equiv 0.5$, denoted by the white lines). The balanced potential (bottom) only performs the recovery of the hyperbolic tangent interface profile. The horizontal lines at $T = 0.50$ correspond to the profiles shown in Fig. 3.

potential ω_b is exactly zero at initialization, it will by definition not affect the circular interface and is therefore identical to the initial condition.

B. Spinodal decomposition

Figure 2 shows the spinodal decomposition on a $[2 \times 2]$ square domain with periodic boundary conditions. This square domain is divided into 25×25 spectral elements, and all boundaries are periodic. At initialization, a mean $C = 0.35$ is set, with variations of 0.01 to trigger the start of the decomposition. The interface thickness is set to $\epsilon = 0.02$, and $M = 1$ is used. Once the solution reaches a steady state (uniform ω), the simulation is stopped. The CH equation (14) will cause a decomposition process, which is advanced in time by a BDF2 time stepping method with a time step of 0.01. Although both chemical potentials achieve a quick spinodal decomposition, their dynamics are quite different. The classic chemical potential performs diffusion by mean curvature, see Eq. (28), a process which only stops once a uniform curvature has been obtained. For infinite time, this implies that all enclosed volumes will merge into a single circular interface (so-called coarsening). In contrast, the balanced chemical potential will only perform the recovery of the equilibrium profile of Eq. (11). At infinite time, it allows the persistence of small features without any coarsening. Note that this diffusion effect may be relevant in some physical processes like Ostwald ripening, and therefore, the proposed energy functional is not directly intended for these cases. Furthermore, as shown in Fig. 3, the balanced chemical potential does not show any bulk diffusion: outside the interface region, it attains the theoretical bulk value of 0 or 1. However, the classic chemical potential has overshoots with respect to the bulk values in these regions.

C. Rising bubble

To test the effect of both chemical potentials under dynamic circumstances, a coupling between the Navier–Stokes (NS) and Cahn–Hilliard (CH) equations[40] is made. The velocity from the NS equations is used to advect the phase-field parameter, and the phase-field parameter is used to determine the local density, viscosity, and surface tension effects due to the presence of the interface in the NS equation. A buoyant bubble inside a $[1 \times 2]$ rectangular domain with no-slip boundary conditions is considered. The rectangular domain is divided into 8×16 spectral elements, and the adaptive mesh refinement will refine the mesh four times around the interface. A reference solution for this problem is available,[41] and all other settings used here can be found in that work. The interface thickness is set to $\epsilon = 0.01$, and $M = 1/2500$ is used. Coupling convergence is declared once the relative norm of the residual is below 10^{-4}. To allow comparison with the sharp interface reference cases, enclosed mass is defined by the following integral:

$$m_{enclosed} = \int_{C \geq 1/2} 1 \, \mathrm{d}V, \tag{29}$$

which can be considered as the enclosed mass in the sharp interface limit. Figure 4 shows that by using the classic chemical potential, about 5% of the enclosed mass is lost (with respect to the theoretical value), while the balanced chemical potential manages to limit this to less than 0.05%. This reduction in the enclosed mass loss for the balanced chemical potential is also an indication of the improvement in the boundedness of C, in contrast to the large over-/undershoots of the classical functional as shown in the previous example. As enclosed mass is conserved implicitly, numerical and approximation errors can cause fluctuations in the enclosed mass conservation. Although small, because of the logarithmic scaling of the vertical axis, these fluctuations are clearly visible in Fig. 4. To indicate the general trend of these fluctuations, a moving average has been added. This line shows that the small errors can accumulate over time in any direction (mass loss and gain). Nevertheless, in time, the enclosed mass loss remains small, especially when compared to the classic chemical potential. A direct consequence of a large enclosed mass loss is visible in Fig. 5, which shows that only the (enclosed mass

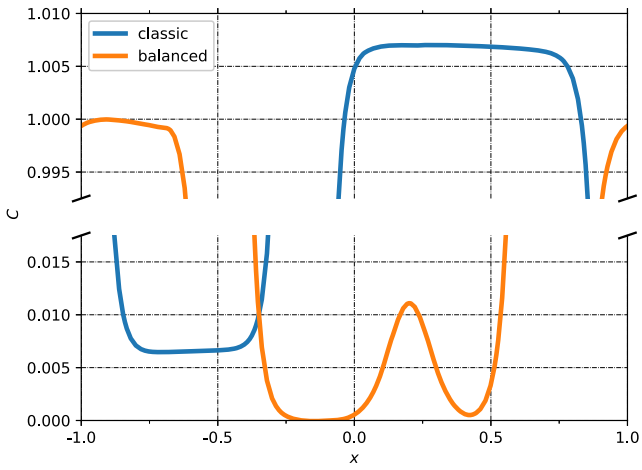

FIG. 3. Extremities of the C profiles at $T = 0.50$ along the horizontal lines shown in Fig. 2. The classic chemical potential does not attain the theoretical values of 0 and 1 in the bulk regions, while the balanced chemical potential does.

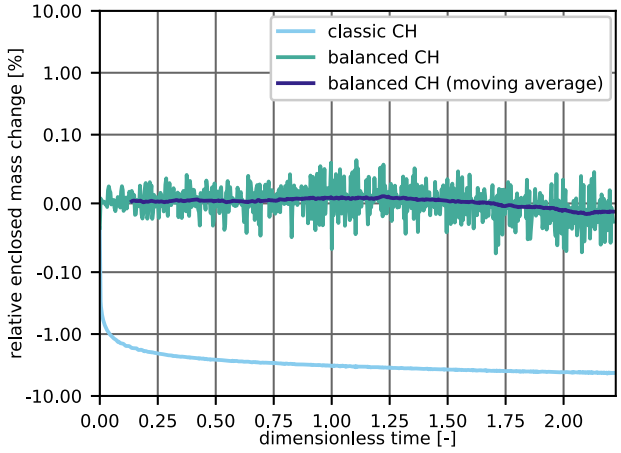

FIG. 4. Relative change of enclosed mass (with respect to the theoretical value) for a rising bubble. While the classic chemical potential (16) loses about 5% of its enclosed mass, the balanced chemical potential (26) is able to conserve the enclosed mass well within 0.05%.

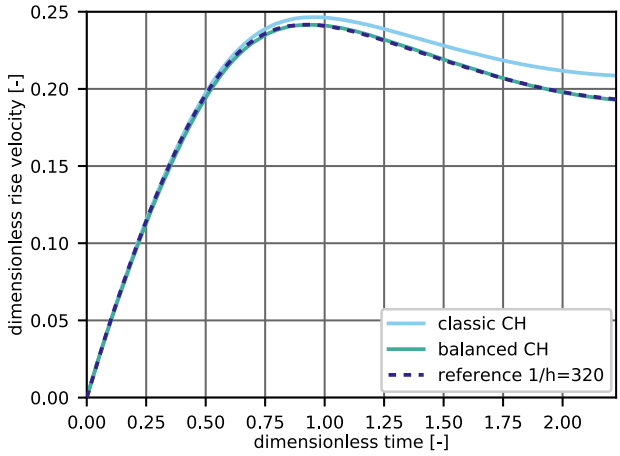

FIG. 5. Dimensionless rise velocity for a bubble with the classic and balanced chemical potentials, compared to a sharp interface reference case.[41] Only the balanced chemical potential matches the reference, showing the importance of conservation of enclosed mass.

conserving) balanced chemical potential is able to reproduce the reference data for the rise velocity of the bubble.

IV. CONCLUSION

This work establishes that the loss of (enclosed) mass and bulk diffusion is caused by an additional mean curvature term in the classic chemical potential (16). Application of this classic chemical potential will lead to a nonphysical motion or diffusion by mean curvature for the AC and CH equations, respectively. From a physical viewpoint, the mean curvature term should be balanced by a pressure term (through the Young–Laplace equation). However, this is not the case for the additional mean curvature term in the classic chemical potential. By a subtle modification in the derivation of the chemical potential, a balanced chemical potential (26) can be derived. This balanced chemical potential removes the nonphysical interface motion (AC) and bulk diffusion (CH) and thereby resolves a long-standing limitation of phase-field methods. Furthermore, while it conserves (enclosed) mass for curved interfaces and is able to model spinodal decomposition, it also improves physical results when applied to two-phase systems.

ACKNOWLEDGMENTS

Funding for this work from the Research Council of Norway under FRIPRO Project No. 275587 is gratefully acknowledged.

APPENDIX A: GRADIENT FLOW DERIVATION

Mathematically, the evolution of the uncoupled (from the NS equation) phase-field $C(\mathbf{x}, t)$ is given by the gradient flow of the energy density $f(C)$,

$$\frac{\partial C}{\partial t} = -\nabla_{\mathcal{H}} f(C). \tag{A1}$$

Here, $\nabla_{\mathcal{H}}$ denotes the Hilbert space gradient of f at C, which ensures that C decreases along the gradient of f on $\mathcal{H}$. The choice of this function space $\mathcal{H}$ affects the behavior of the equation under consideration. Two well known gradient flows are the L^2 and H^{-1} gradient flows. The L^2 gradient flow gives

$$\begin{aligned}\langle \nabla \mathcal{F}(C), \psi \rangle_{L^2} &= \lim_{\gamma \to 0} \frac{\mathcal{F}(C + \gamma\psi) - \mathcal{F}(C)}{\gamma} \\ &= \int_\Omega \frac{\delta \mathcal{F}}{\delta C} \psi \, \mathrm{d}\mathbf{x} \quad \psi \in C_c^\infty(\Omega),\end{aligned} \tag{A2}$$

which results in the Allen–Cahn equation,

$$\frac{\partial C}{\partial t} = -\mu. \tag{A3}$$

The H^{-1} gradient flow gives

$$\begin{aligned}\langle \nabla \mathcal{F}(C), \psi \rangle_{H^{-1}} &= \lim_{\gamma \to 0} \frac{\mathcal{F}(C + \gamma\psi) - \mathcal{F}(C)}{\gamma} \\ &= -\int_\Omega \Delta \frac{\delta \mathcal{F}}{\delta C} \psi \, \mathrm{d}\mathbf{x} \quad \psi \in C_c^\infty(\Omega),\end{aligned} \tag{A4}$$

which results in the Cahn–Hilliard equation,

$$\frac{\partial C}{\partial t} = \Delta \mu, \tag{A5}$$

where Δ is the Laplacian. Here, it has been used that H^{-1} is the dual of H_0^1, for which there is a canonical isomorphism $H_0^1 \simeq H^{-1}$. This isomorphism $H_0^1 \to H^{-1}$ can be viewed as the distributional Laplacian $-\Delta$,

$$\begin{aligned}\langle \nabla \mathcal{F}(C), \psi \rangle_{H^{-1}} &= -\left\langle \Delta^{-1} \nabla \mathcal{F}(C), \Delta^{-1} \psi \right\rangle_{H_0^1} \\ &= -\left\langle \nabla^{-1} \nabla \mathcal{F}(C), \nabla^{-1} \psi \right\rangle_{L^2} \\ &= -\left\langle \Delta^{-1} \nabla \mathcal{F}(C), \psi \right\rangle_{L^2}.\end{aligned} \tag{A6}$$

APPENDIX B: BALANCED CHEMICAL POTENTIAL DERIVATION

The redefined Helmholtz energy functional, given by Eq. (25), reads

$$\mathcal{F}_b = \int_\Omega f_b \, \mathrm{d}V = \int_\Omega \frac{\sigma}{\epsilon} \left(\Psi(C) + \frac{\epsilon^2}{2} (\nabla_n C)^2 \right) \mathrm{d}V, \tag{B1}$$

where ∇_n is the gradient normal to the interface Γ. The unit normal vector of this interface is denoted by $\mathbf{n}_\Gamma$, and $\nabla_n C = \nabla C \cdot \mathbf{n}_\Gamma$. If the variational formulation is applied to this energy functional, consequently,

$$\begin{aligned}\mathcal{F}_b(C+\gamma\psi) &= \frac{\sigma}{\epsilon}\int_\Omega \Psi(C+\gamma\psi) + \frac{\epsilon^2}{2}(\nabla_n C + \gamma\nabla_n\psi)^2\,\mathrm{d}V \\ &= \frac{\sigma}{\epsilon}\int_\Omega \Psi(C) + \gamma\Psi'(C)\,\psi + \frac{\epsilon^2}{2}(\nabla_n C)^2 \\ &\quad + \epsilon^2\gamma\nabla_n C\,\nabla_n\psi + \gamma^2\frac{\epsilon^2}{2}(\nabla_n\psi)^2\,\mathrm{d}V \\ &= \mathcal{F}_b(C) + \frac{\sigma\gamma}{\epsilon}\int_\Omega \Psi'(C)\,\psi + \epsilon^2\,\nabla_n C\,\nabla_n\psi\,\mathrm{d}V + \mathcal{O}(\gamma^2) \\ &= \mathcal{F}_b(C) + \frac{\sigma\gamma}{\epsilon}\int_\Omega \Psi'(C)\,\psi + \epsilon^2\underbrace{\mathbf{n}_\Gamma^T(\nabla C\otimes\nabla\psi)\mathbf{n}_\Gamma}_{\text{Replaced by Eq. (B3)}}\,\mathrm{d}V \\ &\quad + \mathcal{O}(\gamma^2), \end{aligned} \tag{B2}$$

Through integration by parts and application of the divergence theorem, the last part of the volume integral can be replaced by more convenient volume and surface integrals (Green's first identity),

$$\begin{aligned}\int_\Omega \mathbf{n}_\Gamma^T(\nabla C\otimes\nabla\psi)\mathbf{n}_\Gamma\,\mathrm{d}V &= -\int_\Omega \psi\,\mathbf{n}_\Gamma^T(\nabla\otimes\nabla C)\mathbf{n}_\Gamma\,\mathrm{d}V \\ &\quad + \int_\Omega \mathbf{n}_\Gamma^T(\nabla\otimes(\psi\nabla C))\mathbf{n}_\Gamma\,\mathrm{d}V \\ &= -\int_\Omega \psi\,\mathbf{n}_\Gamma^T H(C)\mathbf{n}_\Gamma\,\mathrm{d}V \\ &\quad + \int_\Omega \nabla(\psi\nabla C\cdot\mathbf{n}_\Gamma)\cdot\mathbf{n}_\Gamma\,\mathrm{d}V \\ &= -\int_\Omega \psi\frac{\partial^2 C}{\partial n^2}\,\mathrm{d}V + \oint_{\partial\Omega}\psi\nabla C\cdot\mathbf{n}_s\,\mathrm{d}S, \end{aligned} \tag{B3}$$

where $H(C) = \nabla\otimes\nabla C$ is the Hessian matrix of C, and $\mathbf{n}_s$ is the normal vector of $\partial\Omega$. Next, after neglecting the higher order terms, Eq. (B2) can be rewritten to obtain the directional derivative of $\mathcal{F}_b$,

$$\begin{aligned}&\lim_{\gamma\to 0}\frac{\mathcal{F}_b(C+\gamma\psi)-\mathcal{F}_b(C)}{\gamma} \\ &\quad = \frac{\sigma}{\epsilon}\int_\Omega\left(\Psi'(C) - \epsilon^2\frac{\partial^2 C}{\partial n^2}\right)\psi\,\mathrm{d}V + \sigma\oint_{\delta\Omega}\epsilon\psi\nabla C\cdot\mathbf{n}_s\,\mathrm{d}S. \end{aligned} \tag{B4}$$

Finally, the balanced chemical potential ω_b, which is by definition equal to the functional derivative of $\mathcal{F}_b$, is given by the following relations:

$$\omega_b \equiv \frac{\delta\mathcal{F}_b}{\delta C} = \frac{\sigma}{\epsilon}\left(\Psi'(C) - \epsilon^2\frac{\partial^2 C}{\partial n^2}\right) \quad \text{on } \Omega, \tag{B5}$$

$$\omega_b = \frac{\sigma}{\epsilon}\left(\Psi'(C) - \epsilon^2\frac{\partial^2 C}{\partial n^2}\right) + \sigma\epsilon\nabla C\cdot\mathbf{n}_s \quad \text{on } \partial\Omega. \tag{B6}$$

DATA AVAILABILITY

The data that support the findings of this study are available from the corresponding author upon reasonable request.

REFERENCES

[1] D. Jacqmin, "Contact-line dynamics of a diffuse fluid interface," J. Fluid Mech. **402**, 57–88 (2000).
[2] P. Yue, J. J. Feng, C. Liu, and J. Shen, "A diffuse-interface method for simulating two-phase flows of complex fluids," J. Fluid Mech. **515**, 293–317 (2004).
[3] V. V. Khatavkar, P. D. Anderson, P. C. Duineveld, and H. E. H. Meijer, "Diffuse-interface modelling of droplet impact," J. Fluid Mech. **581**, 97–127 (2007).
[4] J. Wu, C. Liu, and N. Zhao, "Dynamics of falling droplets impact on a liquid film: Hybrid lattice Boltzmann simulation," Colloids Surf., A **472**, 92–100 (2015).
[5] A. Badillo, "Quantitative phase-field modeling for wetting phenomena," Phys. Rev. E **91**, 033005 (2015).
[6] V. E. Badalassi, H. D. Ceniceros, and S. Banerjee, "Computation of multiphase systems with phase field models," J. Comput. Phys. **190**, 371–397 (2003).
[7] G. Soligo, A. Roccon, and A. Soldati, "Mass-conservation-improved phase field methods for turbulent multiphase flow simulation," Acta Mech. **230**, 683–696 (2019).
[8] J. W. Cahn and J. E. Hilliard, "Free energy of a nonuniform system. I. Interfacial free energy," J. Chem. Phys. **28**, 258–267 (1958).
[9] A. A. Wheeler, B. T. Murray, and R. J. Schaefer, "Computation of dendrites using a phase field model," Physica D **66**, 243–262 (1993).
[10] J. A. Warren and W. J. Boettinger, "Prediction of dendritic growth and microsegregation patterns in a binary alloy using the phase-field method," Acta Metall. Mater. **43**, 689–703 (1995).
[11] L. K. Antanovskii, "A phase field model of capillarity," Phys. Fluids **7**, 747–753 (1995).
[12] D. Jasnow and J. Viñals, "Coarse-grained description of thermo-capillary flow," Phys. Fluids **8**, 660–669 (1996).
[13] C. Beckermann, H.-J. Diepers, I. Steinbach, A. Karma, and X. Tong, "Modeling melt convection in phase-field simulations of solidification," J. Comput. Phys. **154**, 468–496 (1999).
[14] W. J. Boettinger, J. A. Warren, C. Beckermann, and A. Karma, "Phase-field simulation of solidification," Annu. Rev. Mater. Res. **32**, 163–194 (2002).
[15] A. Badillo, "Quantitative phase-field modeling for boiling phenomena," Phys. Rev. E **86**, 041603 (2012).
[16] J. van der Waals, "The thermodynamic theory of capillarity under the hypothesis of a continuous variation of density," J. Stat. Phys. **20**, 200–244 (1979), original work published in 1893; translated by J. S. Rowlinson.
[17] J. W. Cahn, "Free energy of a nonuniform system. II. Thermodynamic basis," J. Chem. Phys. **30**, 1121–1124 (1959).
[18] J. W. Cahn and J. E. Hilliard, "Free energy of a nonuniform system. III. Nucleation in a two-component incompressible fluid," J. Chem. Phys. **31**, 688–699 (1959).
[19] J. W. Cahn, "On spinodal decomposition," Acta Metall. **9**, 795–801 (1961).
[20] J. W. Cahn, "Phase separation by spinodal decomposition in isotropic systems," J. Chem. Phys. **42**, 93–99 (1965).
[21] D. Jacqmin, "Calculation of two-phase Navier–Stokes flows using phase-field modeling," J. Comput. Phys. **155**, 96–127 (1999).
[22] P. Yue, C. Zhou, and J. J. Feng, "Spontaneous shrinkage of drops and mass conservation in phase-field simulations," J. Comput. Phys. **223**, 1–9 (2007).
[23] T. Biben and C. Misbah, "Tumbling of vesicles under shear flow within an advected-field approach," Phys. Rev. E **67**, 031908 (2003).
[24] X. Yang, J. J. Feng, C. Liu, and J. Shen, "Numerical simulations of jet pinching-off and drop formation using an energetic variational phase-field method," J. Comput. Phys. **218**, 417–428 (2006).
[25] B. Nestler, F. Wendler, M. Selzer, B. Stinner, and H. Garcke, "Phase-field model for multiphase systems with preserved volume fractions," Phys. Rev. E **78**, 011604 (2008).
[26] Y. Hu, Q. He, D. Li, Y. Li, and X. Niu, "On the total mass conservation and the volume preservation in the diffuse interface method," Comput. Fluids **193**, 104291 (2019).
[27] Y. Wang, C. Shu, J. Y. Shao, J. Wu, and X. D. Niu, "A mass-conserved diffuse interface method and its application for incompressible multiphase flows with large density ratio," J. Comput. Phys. **290**, 336–351 (2015).
[28] Y. Li, J.-I. Choi, and J. Kim, "A phase-field fluid modeling and computation with interfacial profile correction term," Commun. Nonlinear Sci. Numer. Simul. **30**, 84–100 (2016).
[29] Y. Zhang and W. Ye, "A flux-corrected phase-field method for surface diffusion," Commun. Comput. Phys. **22**, 422–440 (2017).

[30]Y. Wang, C. Shu, L. M. Yang, and H. Z. Yuan, "On the re-initialization of fluid interfaces in diffuse interface method," Comput. Fluids **166**, 209–217 (2018).
[31]P. Yue, C. Zhou, J. J. Feng, C. F. Ollivier-Gooch, and H. H. Hu, "Phase-field simulations of interfacial dynamics in viscoelastic fluids using finite elements with adaptive meshing," J. Comput. Phys. **219**, 47–67 (2006).
[32]H. Garcke, "Curvature driven interface evolution," Jahresber. Dtsch. Math.-Ver. **115**, 63–100 (2013).
[33]A. A. Lee, A. Münch, and E. Süli, "Degenerate mobilities in phase field models are insufficient to capture surface diffusion," Appl. Phys. Lett. **107**, 081603 (2015).
[34]Another frequently applied range for C is from $C = -1$ to $C = 1$. Both definitions can be interchanged without affecting the physics, and all derivations in this work are valid for both definitions.
[35]M. Kang, R. P. Fedkiw, and X.-D. Liu, "A boundary condition capturing method for multiphase incompressible flow," J. Sci. Comput. **15**, 323–360 (2000).
[36]J. U. Brackbill, D. B. Kothe, and C. Zemach, "A continuum method for modeling surface tension," J. Comput. Phys. **100**, 335–354 (1992).
[37]A. Novick-Cohen and L. A. Segel, "Nonlinear aspects of the Cahn-Hilliard equation," Physica D **10**, 277–298 (1984).
[38]K. Park, M. Gerritsma, and M. Fernandino, "C1 continuous *h*-adaptive least-squares spectral element method for phase-field models," Comput. Math. Appl. **75**, 1582 (2017).
[39]K. Park, M. Gerritsma, and M. Fernandino, "Numerical solution of Cahn-Hilliard system by adaptive least-squares spectral element method," in *Large-Scale Scientific Computing*, Lecture Notes in Computer Science, edited by I. Lirkov and S. Margenov (Springer International Publishing, 2018), pp. 128–136.
[40]K. Park, C. A. Dorao, and M. Fernandino, "Numerical solution of coupled Cahn-Hilliard and Navier-Stokes system using the least-squares spectral element method," in *Proceedings of the 14th ASME International Conference on Nanochannels, Microchannels, and Minichannels (ICNMM2016)* (American Society of Mechanical Engineers, 2016), p. V01BT33A002.
[41]S. Hysing, S. Turek, D. Kuzmin, N. Parolini, E. Burman, S. Ganesan, and L. Tobiska, "Quantitative benchmark computations of two-dimensional bubble dynamics," Int. J. Numer. Methods Fluids **60**, 1259–1288 (2009).